Available online at www.sciencedirect.com

ScienceDirect

Ceramics International 41 (2015) 10818–10827

CERAMICS INTERNATIONAL

www.elsevier.com/locate/ceramint

Mechanical and tribological properties of hydroxyapatite nanoparticles extracted from natural bovine bone and the bone cement developed by nano-sized bovine hydroxyapatite filler

M.R. Ayatollahi[a,*], Mohd Yazid Yahya[b], H. Asgharzadeh Shirazi[a], Shukur Abu Hassan[b]

[a]*Fatigue and Fracture Research Laboratory, Center of Excellence in Experimental Solid Mechanics and Dynamics, School of Mechanical Engineering, Iran University of Science and Technology, Narmak, 16846-13114 Tehran, Iran*

[b]*Center for composite, Institute for Vehicle System and Engineering, Universiti Teknologi Malaysia, 81310, Johor Bahru Malaysia*

Received 17 March 2015; received in revised form 6 May 2015; accepted 6 May 2015
Available online 14 May 2015

Abstract

The aim of this study is twofold. Firstly, it provides a nano-sized hydroxyapatite derived from bovine bone (BHA), as a raw material and natural source of HA, and to obtain the mechanical and tribological properties of sintered BHA ceramic. Secondly, it evaluates the mechanical and tribological properties of a commercially available bone cement by incorporating nano-sized BHA as a bone compatible nano-filler. In order to achieve these two goals, the mechanical and tribological properties of sintered BHA ceramic and nano-composite cements were measured using nano-indentation and nano-scratch experiments. The results indicated that the nano- hydroxyapatite of single phase with high crystallinity and appropriate mechanical and tribological properties could be produced from the natural bovine bone. Moreover, it was found that the nano-composite with 10 wt% BHA exhibited a good improvement in mechanical and tribological properties in comparison with other examined PMMA/BHA nano-composites.

Keywords: B. Nano-composite; C. Mechanical properties; Hydroxyapatite; Bovine bone; Bone cement

1. Introduction

In the past few decades, considerable research studies have been devoted to the synthesis of various bioceramics. Amongst different classes of bioceramics, hydroxyapatite (HA) $[Ca_{10}(PO_4)_6(OH)_2]$ is the most emerging bioceramic, which is extensively used in various clinical applications such as orthopedics and dentistry. The intense use of HA has been due to its special chemical composition, and also its biological and crystallographic similarity with the mineral portion of hard tissues. There are two main methods for producing HA; the first is inorganic synthesis such as wet-chemical method, sol–gel method and hydrothermal method [1–6]. The other technique is the use of natural sources such as eggshells, cuttlefish shells and bovine bone as the main starting materials to synthesize HA [7–10]. Bovine bone, as a raw material, is a potential source of natural HA which can be a good choice for producing hydroxyapatite powder. This is because as an inexpensive and easily available material, bovine bone is morphologically and structurally similar to human's bone. However, the mechanical and tribological properties of HA obtained from natural sources, especially HA from bovine bone (BHA), have not been fully understood and investigations in this field are still widely open.

Polymethylmethacrylate (PMMA) polymers reinforced by Hydroxyapatite (HA) are among the useful applications of HA which have high potential for improving the biological and physicochemical properties of orthopedic cements. Acrylic or PMMA-based bone cements are widely used in clinical applications for bone cementation and fixation purposes of orthopedic prosthesis. The lack of strong adhesion between the

*Corresponding author. Tel.: +98 21 77240201; fax: +98 21 77240488.
E-mail address: m.ayat@iust.ac.ir (M.R. Ayatollahi).

http://dx.doi.org/10.1016/j.ceramint.2015.05.021
0272-8842/

implant and bone has prompted many investigations in which bone-compatible fillers are incorporated into the acrylic bone cement matrix. Researchers have found that the incorporation of hydroxyapatite into the bone cement matrix can improve the biocompatibility of cement and may also enhance fixation by directly stimulating the hosting bone [11–15]. Despite various potential applications of PMMA/HA composite, limited information is available on the mechanical and tribological properties of HA-reinforced bone cements, especially in the scope of nanomaterials. One of the main features of nano-sized particles is their high surface area to volume ratios. This allows the nanoparticles to provide substantially higher interfacial area for load transfer when incorporated into a composite matrix compared to their micro counterparts.

In this study, two main purposes were pursued; the first goal was to reach a nano-hydroxyapatite derived from natural bovine bone (BHA), as the raw material, and to explore the mechanical behavior of sintered BHA ceramic. The other aim was to evaluate the effect of BHA on the mechanical and tribological properties of the resulting PMMA/BHA nano-composite cements (as an important application of HA). In order to achieve these aims, the mechanical and tribological properties of BHA ceramic and nano-composite cements were measured using nano-indentation and nano-scratch experiments.

2. Materials and methods

2.1. Nano-hydroxyapatite powder preparation

The hydroxyapatite powder was derived from natural bovine bone. The purchased bovine bone was cleaned from visible adhered impurities and waste substances such as joint cartilage, ligaments and tissues stuck on the bone. The cleaned bone was boiled in distilled water for 3 h to make the removal of the bone marrow and tendons easier. After the cleaning process, the clean bone samples were defatted by continuing the boiling in the distilled water. The boiled bone samples were dried in an oven at 100 °C for 24 h in order to avoid soot formation on the surface of the material during the heating treatment. After that, dried specimens were cut into cubic prism shapes (10 mm × 10 mm × 10 mm) and calcined in an electric furnace at 900 °C using a temperature rate of 5 °C/min under ambient condition. The temperature was kept for 2 h in the same degree to remove the organic substances. The samples were cooled until they reach the room temperature by slow furnace cooling and then crashed by mortar pestle into powder. Hereafter, since the molecular purity and mechanical, physical and biological properties of HA are improved by nano-sized hydroxyapatite, the nano-structural powders were produced via a high energy planetary ball mill. Among this procedure, in order to minimize impurities during the milling step, a zirconia cup and balls with a ball-to-powder weight ratio of 6:1 were used.

2.2. Sintered BHA ceramic preparation

The BHA powder was uniaxially pressed in 156 MPa into the green body using a cylindrical die with a 20 mm diameter. The compacted green body was pressurelessly sintered in air atmosphere in temperature of 1200 °C, with a furnace ramp rate of 5 °C/min and dwell time for 2 h. It is worth noting that this temperature was selected based on the recommendations of the previous studies [16–18]. In order to obtain a smooth surface for nano-indentation and nano-scratch tests, the surface of sample was polished with a diamond paste having a mesh size of 1 and 0.5 μm, respectively and the roughness of the sample was checked using atomic force microscopy (AFM).

2.3. Nano-composite sample preparation

EUROFIX GUN® (Low viscosity, Synimed Company, France), as a commercially available bone cement, was purchased to prepare the nano-composite cement samples. The acrylic bone cement is constituted of polymer powder and liquid monomer. The composition of a commercially available bone cement used in this work is listed in Table 1. Moreover, the nano-hydroxyapatite derived from bovine bone (BHA) was selected as bone compatible nano-filler. Weighed amounts of polymer and BHA powders (i.e. 0 wt%, 5 wt%, 10 wt% and 15 wt% of BHA) were mixed with each other using a mixer mill (Retsch MM400, Germany) for 2 min with a vibration frequency of 20 s^{-1}. Vacuum mixing was used to prepare the samples as recommended by other researchers [19,20]. Afterwards, the resulting mixture of polymer and BHA powders with liquid monomer were poured into the vacuum mixing machine and maintained for 15 s under vacuum pressure of 0.7 bars at a temperature of 23 ± 3 °C. The admixture was blended for 30 s and finally held for a further 15 s in the vacuum mixing machine. After mixing the nano-composite components, the mixture dough was injected into each separate cubic mold with dimension of 10 × 10 × 5 mm^3. The nano-composite cement samples were allowed to cure for 15 min in ambient conditions and the samples were subsequently separated from the molds. All samples were grounded with 400–2500 grit sandpapers and after that were polished with an alumina suspension in order to achieve a smooth surface for nano-indentation and nano-scratch tests. The perfect polished samples were kept for two months in the ambient conditions in order to reach to relatively steady state of nano-composite cements before performing nano-indentation and nano-scratch experiments.

2.4. Experiments

The mechanical and tribological properties of the specimens were characterized based on ISO 14577 standard using nano-indentation and nano-scratch test instrument (Triboscope system, Hysitron Inc., USA) equipped with a Berkovich type

Table 1
Composition of commercially available bone cement used in this study.

Powder content (60 g)		Liquid content (30 ml)	
Polymethylmethacrylate	52.56 g	**Methylmethacrylate**	29.64 ml
Benzoyl peroxide	1.44 g	***N,N* Dimethyl p-toluidine**	0.36 ml
Barium sulfate	6.00 g	**Hydroquinone**	18–20 ppm

indenter tip. The Berkovich diamond indenter has an average radius of curvature of about 150 nm so that it is primarily utilized for bulk materials and thin films with thicknesses greater than 100 nm. The calibrated contact area function was derived from indentation tests carried out previously on a standard fused quartz sample using methods recommended by Oliver and Pharr [21]. Eventually, the system was coupled with an AFM (NanoScope E, Digital Instruments, USA) which was utilized to evaluate the surface topography of the samples exposed to the nano-indentation and nano-scratching tests.

2.4.1. Nano-indentation test

In the case of nano-indentation measurement, an indenter tip is pressed into specific locations of the material by applying an increasing normal load. The normal load starts to reduce as the penetration depth of the indenter tip achieves a predefined maximum value and partial or complete relaxation occurs. In this study, the maximum indentation loads of 450 μN and 4000 μN were applied for nano-composite cements and sintered BHA ceramic, respectively. The speed of each loading and unloading step was also kept constant so that the loading and unloading times were set to be 30 s for both steps. Previous research works [22,23] demonstrated that there is a relationship between the penetration depth of indenter and the mechanical properties of materials so that the determined properties will be almost stable for depths greater than 200 nm. In order to reach realistic and acceptable results, the indentation depth should be deep enough to minimize the surface effect, approximately less than 10% of the film thicknesses, as the sample is mounted on a hard substance [24].

Since Oliver–Pharr's method depends on the unloading segment of the load–displacement curve, it assumes that only the elastic displacements are recovered. According to this assumption, an error appears in determination of the mechanical properties of materials due to their time dependent behavior. Based on previous studies, the error in viscous materials would be eliminated at the time which indenter tip is kept at the maximum load for a defined period of time [25,26]. In this work, the maximum load was kept constant for 10 s in order to reduce the creep effects. During the nano-indentation test, load versus displacement is permanently monitored, resulting in a load–displacement curve, shown typically in Fig. 1a. The interaction between the indenter tip and the specimen surface during the indentation process is also plotted in Fig. 1b. Moreover, at least five indentations on the randomly selected points of specimens were performed at ambient conditions.

In the nano-indentation test, during the loading and unloading on a smooth-surface elastic half space, the load and indenter displacement obey power-law relations given as

For loading

$$P = \alpha_1 h^{m_1} \tag{1a}$$

And for unloading

$$P = \alpha (h - h_f)^m \tag{1b}$$

where P and h indicate the indentation load and depth, respectively. h_f also is the depth of residual impression after unloading, and a_1, a, m_1, m are the empirical fitting parameters. The initial slope of the unloading curve is defined as the contact stiffness and denoted as S, which can be determined by differentiating the unloading curve at the peak load (see Fig. 1a):

$$S = \left.\frac{dP}{dh}\right|_{h = h_m} \tag{2}$$

A widely used equation for determining the reduced modulus in the indentation technique has the form

$$S = \frac{2\beta}{\sqrt{\pi}} \times \left(\frac{1}{E_r}\right) \times \sqrt{A} \tag{3a}$$

$$E_r = \frac{\sqrt{\pi}}{2\beta} \times \frac{S}{\sqrt{A}} \tag{3b}$$

where E_r displays the reduced modulus of indentation contact, A is the contact area of the indenter and β is a constant parameter dependent of the indenter's geometry. Consequently, elasticity modulus, as one of the important mechanical properties, can be determined by using nano-indentation results and Sneddon relationship [27] as

$$\frac{1}{E_r} = \frac{1-\nu^2}{E} + \frac{1-\nu_i^2}{E_i} \tag{4}$$

where E and ν represent the elasticity modulus and Poisson's ratio of the sample, E_i and ν_i are the elasticity modulus and Poisson's ratio of indenter tip. In addition, it is considered that $\nu = 0.27$ (for BHA ceramic) [28] and 0.3 (for nano-composite cements) [29], $\nu_i = 0.07$ and $E_i = 1140$ GPa. The used values of ν_i and E_i are based on technical data available for the related Triboscope system.

The normal hardness, as another important mechanical property, can be measured in the nano-indentation test based on Briscoe et al. [30] as

$$H_N = \frac{P_{max}}{A} \tag{5}$$

where P_{max} displays the maximum indentation load and A is the projected area of the contact surface between the specimen and the indenter. Fig. 2 illustrates the AFM images of indentation hole on the sintered BHA ceramic and one of the nano-composite cement samples.

2.4.2. Nano-scratch test

The nanoscratching tests were performed by dragging the indenter tip under a progressive load of fixed loading rate while it was in contact with the specimen's surface. In this study, the maximum normal loads were 450 μN and 4000 μN for nano-composite cements and sintered BHA ceramic, respectively. The length of the scratch was also selected to be 4 μm with a constant scratching speed of 0.13 $\mu m.s^{-1}$. Each specimen was scratched three times in order to attain reliable results. Moreover, AFM images were taken before and after each experiment in order to analyze the sample deformation at the scratch site.

The scratch hardness and the scratch residual depth are good indicators which can give us some useful information about the material resistance in response to the scratch deformation. These parameters can be explored by nano-indentation test.

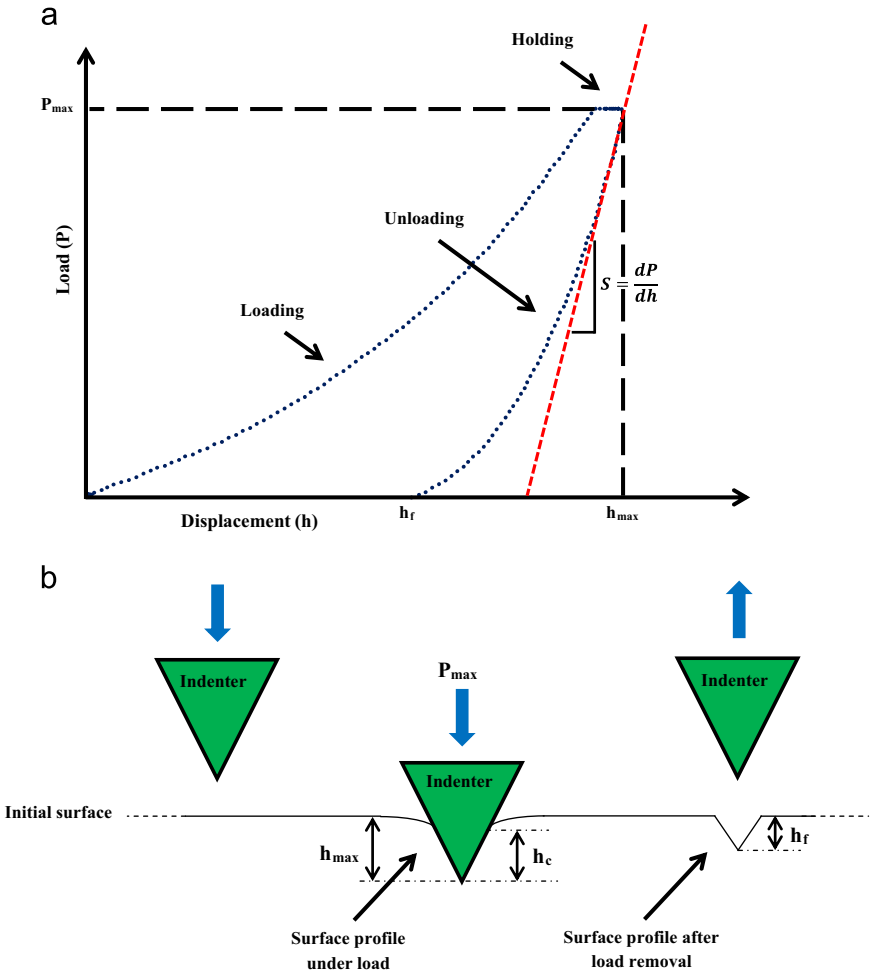

Fig. 1. Schematic of (a) load–displacement curve of nano-indentation experiment and (b) interaction between indenter tip and sample (P_{max}=maximum applied load; h_{max}=maximum penetration depth; h_c=contact depth; h_f=final depth; S=unloading stiffness).

The scratch hardness could be calculated as [31]

$$H_S = 2.31\frac{P'_{max}}{d^2} \quad (6)$$

where P'_{max} indicates the maximum normal load applied on the indenter in the nano-scratch experiment and d displays the residual scratch width. The values of residual scratch width (d) were determined via the AFM images of the scratch sites and the NanoScope V5.12r2 software. Fig. 3 shows the AFM images of the scratch trace for one of the nano-composite cement samples.

3. Results and discussion

3.1. BHA powder characterization

Bovine bone is a composite material consisting of a mineral phase (hydroxyapatite), collagen, non-collagenous proteins, lipids, and water. The infrared spectrum of bone reported by Boskey and Camacho indicates the presence of major inorganic species, phosphate (from the mineral hydroxyapatite), carbonate (from carbonate substitution for hydroxyl and phosphate groups), and also the organic components such as amide functional groups from the protein constituents of bone, i.e., collagen [32]. Ooi et al. [7] have shown that the organic compounds are completely removed from the bone matrices when the bovine bone is annealed at temperatures above 700 °C. They reported that the inorganic phases of annealed bovine bone are composed mainly of Ca and P as the major constituents with some minor components comprising of Na, Mg, O and C. The Ca/P ratio of as-received bovine bone was 2.23 and decreased to about 1.95 when it was annealed at 900 °C. Moreover, it was found that the annealing process enhanced the crystallinity of HA phase in the bone matrix with no secondary phase formation when annealed between 600 °C and 1000 °C. The XRD analysis of the synthesized BHA powder in this study as shown in Fig. 4 exhibited peaks within the 2θ range from 10° to 80° that corresponds to stoichiometric HA (JCPDS 9-432). According to this figure, there was no phase decomposition of BHA into secondary phases such as a-TCP, b-TCP, TTCP or CaO. Royer et al. [33] and Wang et al. [34] reported that the decomposition of HA starts at about 1250–1300 °C, accompanying with deterioration of mechanical properties of HA ceramics. Jarcho et al. [35] have also mentioned that decomposed products would identify at grain boundaries of HA when sintered in air at 1250 °C for 1 h. As shown in Fig. 4, the XRD signatures of BHA powder

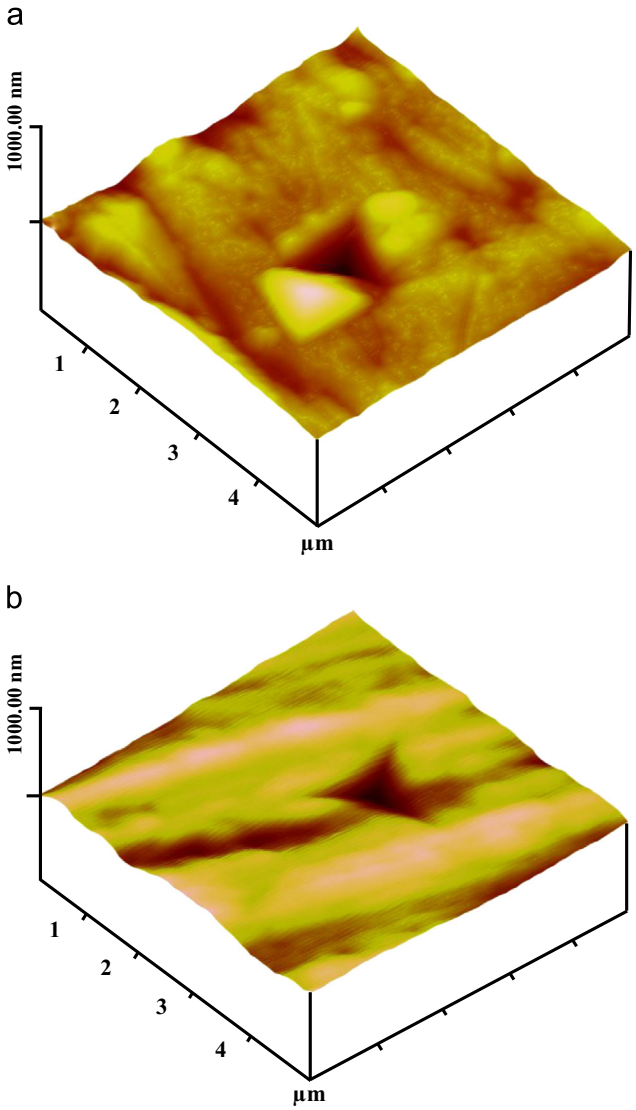

Fig. 2. The AFM image of an indentation hole on the (a) sintered BHA ceramic and (b) one of the nano-composite cement samples.

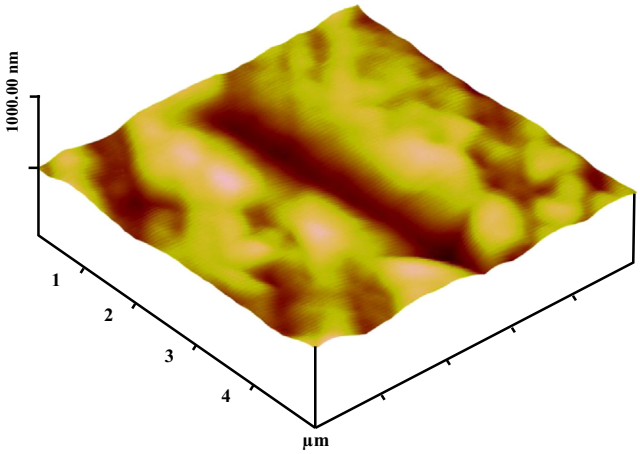

Fig. 3. The AFM images of a scratch trace for one of the nano-composite cement samples.

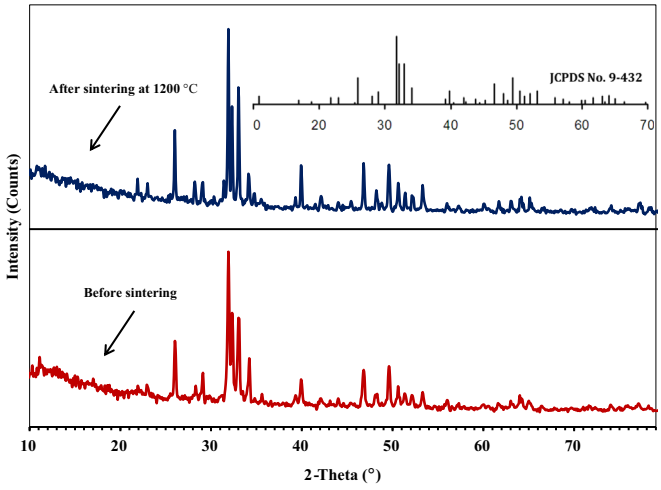

Fig. 4. XRD pattern of BHA obtained from heated bovine bone at 900 °C and correspond to the characteristic peak of HA (JCPDS no. 9-432).

conform to the stoichiometric HA profile and it can be observed that BHA powder production method leads to high crystallinity and single phase HA. On the other hand, the intensity of the major peak of the sintered BHA powder (at 1200 °C) has a vivid increase in comparison with XRD analysis of sample before sintering. In other words, the XRD signatures of BHA sintered at 1200 °C exhibit a substantial increase in peak height which indicates the increase of powder's crystallinity. Estimations of the crystal size from the peak broadening using the Debye–Scherrer formula [36] for the obtained BHA powder was calculated to be about 30 nm. Moreover, the nano-crystalline nature of the derived BHA powder was confirmed by SEM as shown in Fig. 5. This result has an acceptable coincidence with XRD analysis, which reveals that the particles are very small i.e. in the nanometer size range.

3.2. Sintered BHA ceramic results

In this study, the mechanical and tribological properties of nano-hydroxyapatite derived from bovine bone were evaluated using nano-indentation and nano-scratch experiments performed on the sintered BHA body sample. Table 2 presents the mean values and the standard deviations of mechanical and tribological properties of the sintered BHA ceramic. According to this table, the elasticity modulus and hardness of sintered BHA ceramic are equal to 141.9 GPa (with standard deviation of 13.9) and 2.232 GPa (with standard deviation of 0.192), respectively. The scratch hardness and the residual scratch depth obtained from the nano-scratch test are also equal to 2.276 GPa (with standard deviation of 0.330) and 109.1 nm (with standard deviation of 8.8), respectively. It is noteworthy to know that residual scratch depth and scratch resistance are in contrary to each other, that is the lower the residual scratch depth, the higher the scratch resistance of the material. The values of mechanical and tribological properties determined in this study for sintered HA ceramic are in the range of properties reported in previous papers [7,8,25–28]. Karimzadeh et al. [18] evaluated the effect of sintering temperature (at various temperatures between 1000–1400 °C) on the mechanical and tribological properties of a commercial nanohydroxyapatite (HAc) by nano-indentation and nano-scratch experiments.

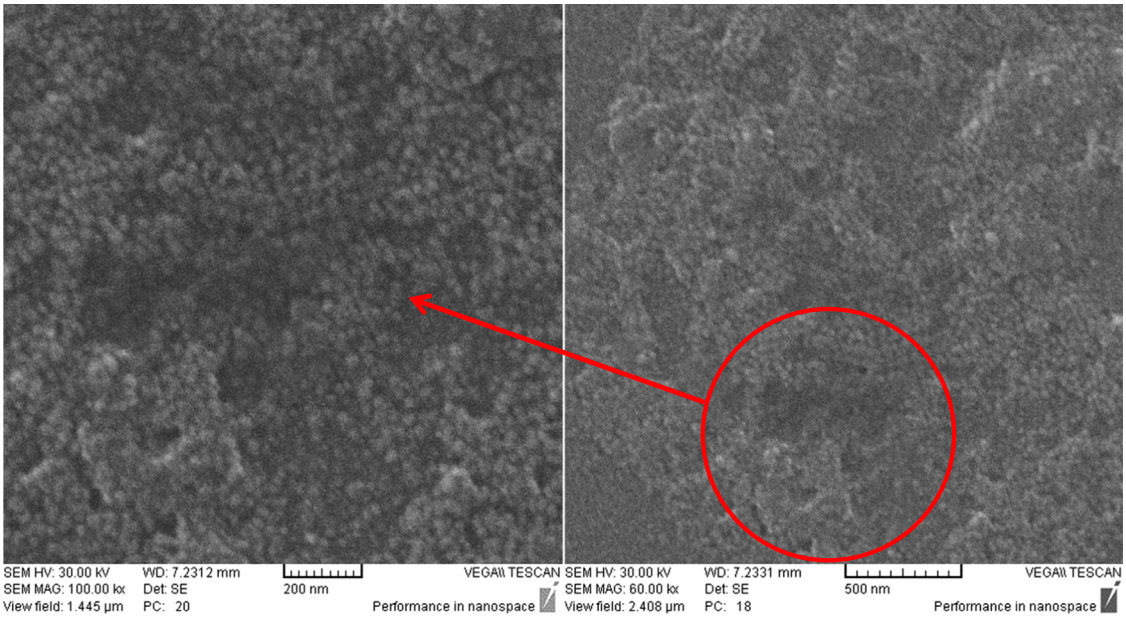

Fig. 5. SEM images of nano-hydroxyapatite derived from bovine bone in this work.

Table 2
Mechanical and tribological properties of sintered BHA ceramic.

Sample	Mechanical properties		Tribological properties	
	Elasticity modulus (GPa)	Normal hardness (GPa)	Scratch hardness (GPa)	Residual scratch depth (nm)
Sintered BHA ceramic	141.944 ± 13.956	2.232 ± 0.192	2.276 ± 0.330	109.146 ± 8.831

According to their results, the highest value of elasticity modulus was found to be 153 ± 9.6 GPa for the HAc specimen sintered at 1200 °C and the lowest one was equal to 48 ± 7.9 GPa for the specimen sintered at 1000 °C. The maximum and minimum hardness values of HAc samples were also 7 ± 0.7 GPa and 1 ± 0.6 GPa at the sintering temperatures of 1300 °C and 1000 °C, respectively. Moreover, the lowest values of residual scratch depth and scratch hardness were equal to 108 ± 5 nm, 1 ± 0.8 GPa for HAc samples sintered at 1000 °C and the highest values were 192 ± 7 nm, 8 ± 0.4 GPa for samples sintered at 1300 °C. In a similar study, Herliansyah et al. [8] investigated the effect of sintering temperature on the hardness of sintered micro-BHA body. They reported that the lowest hardness value of 0.311 GPa was determined for the sample sintered at 1000 °C, whereas the maximum hardness value of 2.403 GPa was measured for the sample sintered at 1300 °C. In addition, the hardness value for the sample sintered at 1200 °C was about 1.5 GPa. The discrepancy between the values of hardness obtained in the present work and in Ref. [8] could be attributed to the difference in the particle size, crystallinity, nature of the starting synthesized powder, relative humidity in the sintering atmosphere and the method of measurement. For example, regarding the measurement method, Qian et al. [37] have illustrated that the nano-indentation hardness can be about 10–30% larger than the micro-hardness for the measured materials. They reported that the main reason for the difference between the results of nano and micro-scale measurements is related to the analysis of the nano-indentation hardness using the projected contact area at peak load instead of the residual projected area. The other reason can be the assumption of purely elastic contact for the elastic/plastic process of indentation [37]. Therefore, the existence of such differences in the values of mechanical and tribological properties in various studies is acceptable and reasonable.

3.3. Nano-composite cements results

In the present work, the nano-hydroxyapatite derived from bovine bone (BHA) was incorporated into a commercial acrylic bone cement as an application of nano-hydroxyapatite (i.e. a bone compatible nano-filler). The mechanical and tribological properties of the resulting nano-composite were experimentally measured by using nano-indentation and nano-scratch measurements. Fig. 6 shows the continuous load versus displacement for five nano-indentation tests conducted on one of the cement samples where a good repeatability of the curves is found in this figure. Similar repeatability was also observed for the results of other specimens in response to nano-indentation test. Fig. 7 displays the mean values and the standard deviations of the elasticity modulus and normal hardness obtained for nano-composite cements. According to this figure, the highest value of elasticity modulus

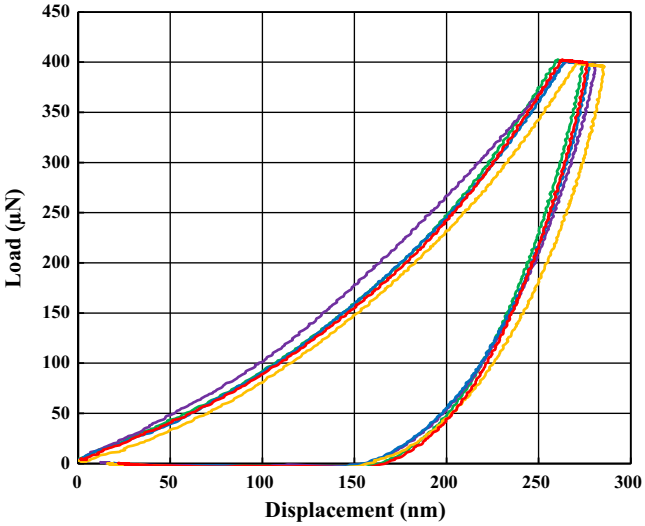

Fig. 6. Load–displacement curves obtained from the nano-indentation tests performed on the nano-composite cement samples of 5 wt% BHA.

is for pure cement sample (i.e. 0 wt% BHA) which equals 4.386 GPa (with standard deviation of 0.400). The maximum normal hardness is related to 10 wt% BHA nano-composite samples that is 0.206 GPa (with standard deviation of 0.023). Moreover, Fig. 8a illustrates the average values and the standard deviations of the scratch hardness measured for nano-composite cements. According to this figure, the maximum mean value of scratch hardness is equal to 0.695 GPa (with standard deviation of 0.077) for a sample with 10 wt% BHA. The scratch residual depth is another tribological property which can be measured by analyzing AFM images before and after the scratch deformation obtained by the nano-scratch test. The longitudinal scratch sections obtained from AFM images before and after scratch deformation for one of the nano-composite cement samples are depicted in Fig. 9. In fact, the scratch residual depth can be determined by measuring the difference between the magnitudes before and after the scratch deformation (see Fig. 9). Fig. 8b shows the mean values and the standard deviations of the residual scratch depth for nano-composite cement samples. Based on this figure, the minimum residual scratch depth is equal to 57.382 nm (with standard deviation of 2.843) for the sample of 10 wt% BHA. Since a lower residual scratch depth indicates a higher scratch resistance of the material and vice versa, therefore, the maximum scratch resistances occurs for the sample of 10 wt. % BHA. Finally, Fig. 10 indicates the transverse sections of the scratch in the nano-composite cement samples which exhibits an acceptable coincidence with the results presented in Fig. 8.

One may expect to obtain the same values for normal Hardness H_N and scratch hardness H_S according to the definition of hardness, i.e. the resistance of material against surface deformation. The difference in mechanisms involved in these two test methods, i.e. nano-indentation and nano-scratch experiments, may be considered as reasons for difference in the values of H_S and H_N. The difference between H_N and H_S can be low (e.g. for BHA ceramic as described in Section 3.2) or high (e.g. for nano-composite cements) depending on the type of material. The normal hardness is the resistance of the material against the local

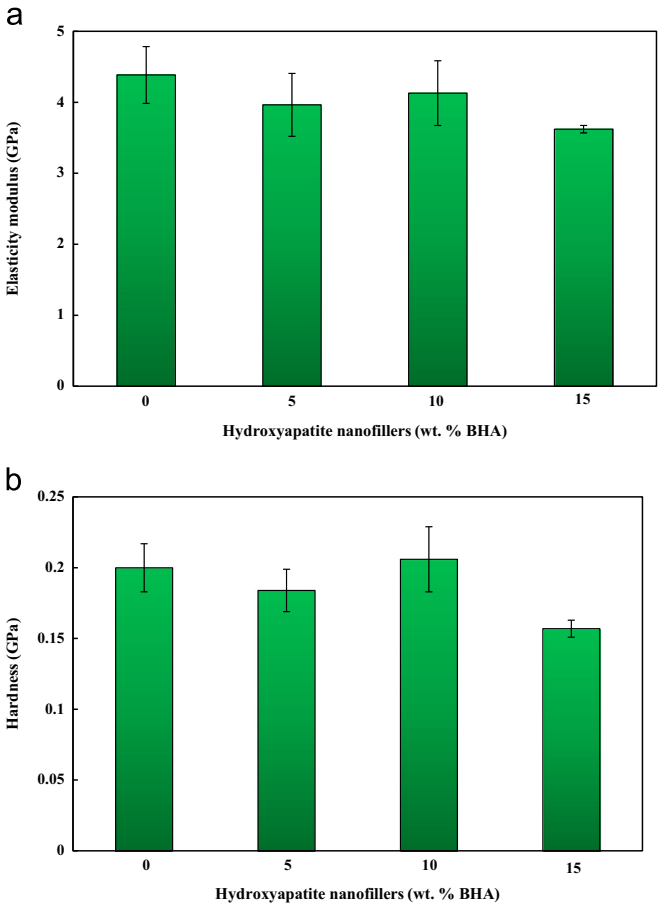

Fig. 7. The mean values and the standard deviations of the (a) elasticity modulus and (b) normal hardness obtained for nano-composite cements.

deformation created via penetrating an indenter vertically, close to static condition, which is determined from nano-indentation test [20]; while the scratch hardness is the response of material under the dynamic deformation of the surface, i.e. plowing deformation, which is caused by the interfacial friction between the indenter and the material. During the dynamic deformation of the surface in the nano-scratch process, the indenter moves laterally and the net energy for causing deformation on the material surface is calculated from the scratch force or the tangential component of the load [45]. The scratch force changes by the mechanism of material deformation and the interfacial friction between the indenter and the material. Therefore, the higher values of scratch hardness relative to the normal hardness can represent the increased resistance of material against the indenter movement.

As shown in Figs. 7 and 8, there are similar trends in the mechanical and tribological properties for nano-composite samples. According to these figures, adding a small amount of nano-hydroxyapatite (5 wt% BHA) to the acrylic bone cement leads to the reduction of mechanical and tribological properties of nano-composite cement in comparison with the pure cement. However, by increasing the amount of the nano-hydroxyapatite up to 10 wt % BHA, these properties increase such that the normal hardness, the scratch hardness and the scratch resistance reach up to their maximum values compared to other samples. Moreover, in the case of 10 wt% BHA, the elasticity modulus exhibits the highest

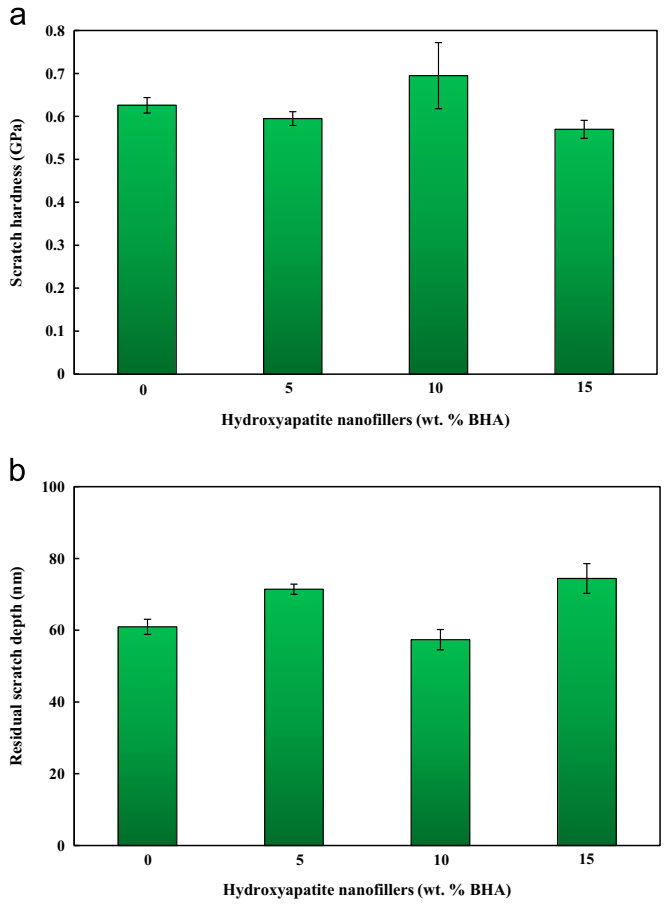

Fig. 8. The mean values and the standard deviations of the (a) scratch hardness and (b) residual scratch depth measured for nano-composite cements.

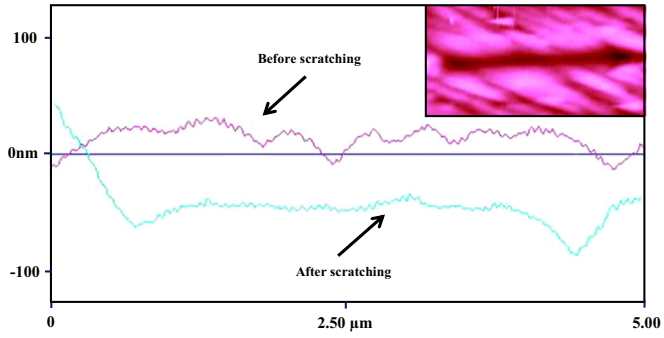

Fig. 9. AFM images before and after scratch deformation for one of the nano-composite cement specimens.

value amongst the PMMA/BHA nano-composite samples. By further addition of BHA up to 15 wt%, the mechanical and tribological properties of cement reduce. Previous studies have suggested that this behavior of PMMA/HA composite can be explained by the role of HA particles in the composite structure [11,38–40]. When a small amount of HA particles are distributed homogeneously, the HA particles behave as load carriers, leading to enhancement of the mechanical and tribological properties. However, when the proportion of the HA particles increases, a nonhomogeneous distribution can occur, resulting in aggregation of particles with poor adhesion to the matrix and leading to a

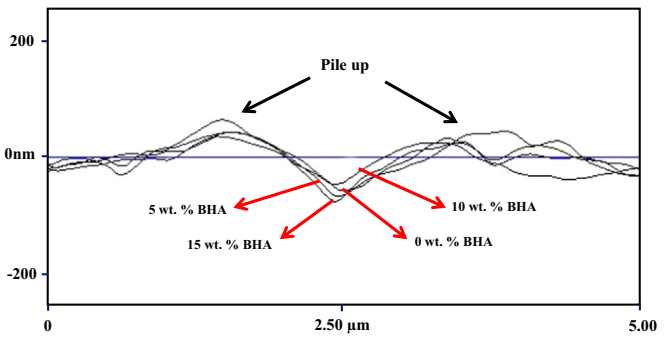

Fig. 10. The transverse sections of the scratches generated in the nano-composite cement specimens.

reduction in the mechanical and tribological properties [11,38–40]. The results obtained in the present work are also consistent with those reported earlier such that the mechanical and tribological properties of nano-composite cement increase by incorporating BHA nano-particles up to a certain percentage, i.e. 10 wt%, and further addition of BHA decreases these properties. Nevertheless, incorporation of a small amount of nano-hydroxyapatite into the bone cement matrix at the beginning leads to the reduction of mechanical and tribological properties of nano-composite cement compared to the pure cement. This reduction can be attributed to the mixing method and polymeric cement structure, as observed and reported in other studies too [40–43]. In other words, the mixing of the filler with the highly viscous polymer/monomer mixture can entrap air causing a decrease in mechanical and tribological properties [40,41]. In addition, the grinding and mixing PMMA-HA powder via ball mill machine may also decrease the properties of PMMA/HA nano-composite, especially when particles are very small e.g. in the range of nanometer size [42,43]. Therefore, these two factors can be the main reasons for a relative reduction in mechanical and tribological properties of bone cement when very small amount of BHA is initially incorporated into the PMMA cement matrix.

As described above, the processing techniques can be of considerable effects on the mechanical properties of nanocomposite. Therefore, it would be useful to review different techniques proposed in the past for possible improvement of the production procedure in order to achieve better properties from the nanocomposite. Previous studies have reported that the mechanical and tribological properties of filled cements depend on a number of factors such as matrix chemical composition, filler type, and filler concentration. Morita et al. [11] indicated that the use of a methyl methacrylate (MMA) monomer containing 4-methacryloyloxyethyl trimellitate anhydride (4-META), as an adhesion promoting agent, can increase the mechanical properties of PMMA/HA cement due to improvement of adhesion between the HA particles and the matrix. Morejón et al. [40] showed that a good adhesion between the HA filler and the cement matrix can be achieved by coating a silane agent on the HA powder which promote the mechanical properties of PMMA/HA cement composite subsequently. They also illustrated that a better adhesion at the HA/polymer interface can be obtained in the cements filled with heated HA powder, and this causes the heated HA-filled

cements to present higher mechanical properties than the cements filled with unheated HA powder. Moreover, previous research studies have shown that the mixing homogeneity of powders, which depend on the powder mixer, medium and mixing procedure, has a significant influence on the properties of composites [43,44]. The papers reviewed above indicate that the potential techniques for improving the mechanical and tribological properties of PMMA/HA composites have not been fully understood and studies in this area are still widely open. Therefore, more investigations are needed to promote the mechanical and tribological properties of developed bone cements by incorporating HA, especially HA nanoparticles derived from natural sources such as bovine bone (BHA). These investigations may concentrate on the manufacturing process, the matrix chemical composition, the size of HA particle and the uniform dispersion of HA within the cement in order to achieve more improvement in terms of mechanical and tribological properties of PMMA/HA composites.

Overall, since the biocompatibility, bioactivity and osteoconductivity of BHA are well-established, this biomaterial can be used in medical and clinical applications, especially in orthopedics and dentistry, but further investigations are still needed to improve its mechanical and tribological properties.

4. Conclusion

In the present work, the nano-hydroxyapatite was successfully produced from natural bovine bone and the obtained BHA, as a bone compatible nano-filler, was homogeneously incorporated into the acrylic bone cement matrix. It was found that:

1- The nano-hydroxyapatite with high purity can be achieved from bovine bone as a raw material and natural source of HA.
2- The XRD profile of the BHA powder has a good coincidence with the stoichiometric HA which shows the BHA powder production method could result in high crystallinity and single phase HA. Moreover, SEM images and XRD analysis indicated that the particle sizes were very small i.e. in the nanometer range.
3- The XRD signatures of BHA sintered at 1200 °C exhibit a vivid increase in peak height in comparison with BHA powder before sintering, indicating that the crystallinity of powder has increased.
4- For all samples, the scratch hardness values determined from the nano-scratch test were higher than the normal hardness obtained from the nano-indentation test. The difference between H_S and H_N was low for sintered BHA ceramic but noticeably high for nano-composite cements. However, the trends of hardness results versus the amount of BHA nano-filler for nano-composite cements were similar in both test methods.
5- The results suggested that the amount of 10 wt% BHA, as a bone-compatible nano-filler, could provide good improvements in the mechanical and tribological properties of PMMA/BHA bone cement nano-composite.

References

[1] M. Fathi, A. Hanifi, Evaluation and characterization of nanostructure hydroxyapatite powder prepared by simple sol–gel method, Mater. Lett. 61 (2007) 3978–3983.
[2] B. Cengiz, Y. Gokce, N. Yildiz, Z. Aktas, A. Calimli, Synthesis and characterization of hydroxyapatite nanoparticles, Colloids. Surf., A 322 (2008) 29–33.
[3] N. Monmaturapoj, Nano-size hydroxyapatite powders preparation by wet-chemical precipitation route, J. Metals Mater. Miner. 18 (2008) 15–20.
[4] M.C. Wang, H.T. Chen, W.J. Shih, H.F. Chang, M.H. Hon, I.M. Hung, Crystalline size, microstructure and biocompatibility of hydroxyapatite nanopowders by hydrolysis of calcium hydrogen phosphate dehydrate (DCPD), Ceram. Int. 41 (2015) 2999–3008.
[5] C. Randorn, A. Kanta, K. Yaemsunthorn, G. Rujijanakul, Fabrication of dense biocompatible hydroxyapatite ceramics with high hardness using a peroxide-based route: a potential process for scaling up, Ceram. Int. 41 (2015) 5594–5599.
[6] F. Bakan, O. Laçin, H. Sarac, A novel low temperature sol–gel synthesis process for thermally stable nano crystalline hydroxyapatite, Powder Technol. 233 (2013) 295–302.
[7] C. Ooi, M. Hamdi, S. Ramesh, Properties of hydroxyapatite produced by annealing of bovine bone, Ceram. Int. 33 (2007) 1171–1177.
[8] M. Herliansyah, M. Hamdi, A. Ide-Ektessabi, M. Wildan, J. Toque, The influence of sintering temperature on the properties of compacted bovine hydroxyapatite, Mater. Sci. Eng. C 29 (2009) 1674–1680.
[9] S. El Asri, A. Laghzizil, A. Saoiabi, A. Alaoui, K. El Abassi, M. hamdi, et al., A novel process for the fabrication of nanoporous apatites from Moroccan phosphate rock, Colloids Surf. A 350 (2009) 73–78.
[10] P. Kamalanathan, S. Ramesh, L.T. Bang, A. Niakan, C.Y. Tan, J. Purbolaksono, H. Chadran, W.D. Teng, Synthesis and sintering of hydroxyapatite derived from eggshells as a calcium precursor, Ceram. Int. 40 (2014) 16349–16359.
[11] S. Morita, K. Furuya, K. Ishihara, N. Nakabayashi, Performance of adhesive bone cement containing hydroxyapatite particles, Biomaterials 19 (1998) 1601–1606.
[12] A.M. Moursi, A.V. Winnard, P.L. Winnard, J.J. Lannutti, R. Seghi, Enhanced osteoblast response to a polymethylmethacrylate–hydroxyapatite composite, Biomaterials 23 (2002) 133–144.
[13] M.J. Dalby, L. Di Silvio, E.J. Harper, W. Bonfield, Initial interaction of osteoblasts with the surface of a hydroxyapatite-poly(methylmethacrylate) cement, Biomaterials 23 (2001) 1739–1747.
[14] M.J. Dalby, L. Di Silvio, E.J. Harper, W. Bonfield, Increasing hydroxyapatite incorporation into poly(methylmethacrylate) cement increases osteoblast adhesion and response, Biomaterials 23 (2002) 569–576.
[15] T.N. Opara, M.J. Dalby, L. Di Silvio, E.J. Harper, W. Bonfield, The effect of varying percentage hydroxyapatite in poly(ethylmethacrylate) bone cement on human osteoblast-like cells, J. Mater. Sci.: Mater. Med. 14 (2003) 277–282.
[16] S. Ramesh, K. Aw, R. Tolouei, M. Amiriyan, C. Tan, M. Hamdi, et al., Sintering properties of hydroxyapatite powders prepared using different methods, Ceram. Int. 39 (2013) 111–119.
[17] S. Ramesh, C.Y. Tan, R. Tolouei, M. Amiriyan, J. Purbolaksono, I. Sopyan, et al., Sintering behavior of hydroxyapatite prepared from different routes, Mater. Des. 34 (2012) 148–154.
[18] A. Karimzadeh, M.R. Ayatollahi, A. Bushroa, M. Herliansyah, Effect of sintering temperature on mechanical and tribological properties of hydroxyapatite measured by nanoindentation and nanoscratch experiments, Ceram. Int. 40 (2014) 9159–9164.
[19] G. Lewis, G. Ed Austin, Mechanical properties of vacuum-mixed acrylic bone cement, J. Appl. Biomater. 5 (1994) 307–314.
[20] A. Karimzadeh, M.R. Ayatollahi, Investigation of mechanical and tribological properties of bone cement by nano-indentation and nanoscratch experiments, Polymer. Test. 31 (2012) 828–833.
[21] W.C. Oliver, G.M. Pharr, Measurement of hardness and elastic modulus by instrumented indentation: advances in understanding and refinements to methodology, J. Mater. Res. 19 (01) (2004) 3–20.

[22] Y. Hu, L. Shen, H. Yang, M. Wang, T. Liu, T. Liang, et al., Nanoindentation studies on Nylon 11/clay nanocomposites, Polymer. Test. 25 (2006) 492–497.
[23] T. Liu, I.Y. Phang, L. Shen, S.Y. Chow, W.D. Zhang, Morphology and mechanical properties of multiwalled carbon nanotubes reinforced nylon-6 composites, Macromolecules 37 (2004) 7214–7222.
[24] A.Y. Jee, M. Lee, Comparative analysis on the nanoindentation of polymers using atomic force microscopy, Polymer. Test. 29 (2010) 95–99.
[25] T. Chudoba, F. Richter, Investigation of creep behaviour under load during indentation experiments and its influence on hardness and modulus results, Surf. Coat. Technol. 148 (2001) 191–198.
[26] A. Ngan, H. Wang, B. Tang, K. Sze, Correcting power-law viscoelastic effects in elastic modulus measurement using depth-sensing indentation, Int. J. Solid Struct. 42 (2005) 1831–1846.
[27] I.N. Sneddon, The relation between load and penetration in the axisymmetric Boussinesq problem for a punch of arbitrary profile, Int. J. Eng. Sci. 3 (1965) 47–57.
[28] X. Fan, E. Case, M. Baumann, The effect of indentation-induced microcracks on the elastic modulus of hydroxyapatite, J. Mater. Sci. 47 (2012) 6333–6345.
[29] B. Murphy, P. Prendergast, Measurement of non-linear microcrack accumulation rates in polymethylmethacrylate bone cement under cyclic loading, J. Mater. Sci.: Mater. Med. 10 (1999) 779–781.
[30] B. Briscoe, P. Evans, S. Biswas, S. Sinha, The hardnesses of poly (methylmethacrylate), Tribology. Int. 29 (1996) 93–104.
[31] J. Williams, Analytical models of scratch hardness, Tribology. Int. 29 (1996) 675–694.
[32] A. Boskey, N.P. Camacho, FT-IR imaging of native and tissue engineered bone and cartilage, Biomaterials 28 (2007) 2456–2478.
[33] A. Royer, J. Viguie, M. Heughebaert, J. Heughebaert, Stoichiometry of hydroxyapatite: influence on the flexural strength, J. Mater. Sci: Mater. Med. 4 (1993) 76–82.
[34] P.E. Wang, T. Chaki, Sintering behaviour and mechanical properties of hydroxyapatite and dicalcium phosphate, J. Mater. Sci: Mater. Med. 4 (1993) 150–158.
[35] M. Jarcho, C. Bolen, M. Thomas, J. Bobick, J. Kay, R.H. Doremus, Hydroxylapatite synthesis and characterization in dense polycrystalline form, J. Mater. Sci. 11 (1976) 2027–2035.
[36] B. Cullity, S. Stock, Elements of X-Ray Diffraction, third ed., Prentice Hall, Inc., 2001.
[37] L. Qian, M. Li, Z. Zhou, H. Yang, X. Shi, Comparison of nano-indentation hardness to microhardness, Surf. Coat. Technol 195 (2005) 264–271.
[38] K. Serbetci, F. Korkusuz, N. Hasirci, Thermal and mechanical properties of hydroxyapatite impregnated acrylic bone cements, Polymer. Test 23 (2004) 145–155.
[39] S.B. Kim, Y.J. Kim, T.L. Yoon, S.A. Park, I.H. Cho, E.J. Kim, I.A. Kim, J.W. Shin, The characteristics of a hydroxyapatite–chitosan–PMMA bone cement, Biomaterials 25 (2004) 5715–5723.
[40] L. Morejón, A.E. Mendizábal, J.A.D. García-Menocal, M.P. Ginebra, C. Aparicio, F.J.G. Mur, et al., Static mechanical properties of hydroxyapatite (HA) powder-filled acrylic bone cements: effect of type of HA powder, J. Biomed. Mater. Res. B: Appl. Biomater. 72 (2005) 345–352.
[41] L.E. Nielsen, R.F. Landel, Mechanical Properties of Polymers and Composites, second ed., Marcel Dekker, New York, 1993.
[42] S.M. Zebarjad, S.A. Sajjadi, T.E. Sdrabadi, A. Yaghmaei, B. Naderi, A study on mechanical properties of PMMA/Hydroxyapatite nanocomposite, Engineering 3 (2011) 795–801.
[43] W.L. Tham, W.S. Chow, Z.A. IShak, Flexural and morphological properties of poly(methyl methacrylate)/hydroxyapatite composites: effects of planetary ball mill grinding time, J. Reinf. Plast. Compos. 29 (2010) 2065–2075.
[44] D. Wei, R. Dave, R. Pfeffer, Mixing and characterization of nanosized powders: an assessment of different techniques, J. Nanopart. Res. 4 (2002) 21–41.
[45] B.J. Briscoe, P.D. Evans, E. Pellilo, S.K. Sinha, Scratching maps for polymers, Wear 200 (1996) 137–147.